RSC Advances

PAPER

View Article Online
View Journal | View Issue

Cite this: *RSC Adv.*, 2024, **14**, 22113

In vitro evaluation and *in situ* intestinal absorption characterisation of paeoniflorin nanoparticles in a rat model

Yifei Xiao,[a] Qidong Wei,[a] Lixin Du,[a] Zhihua Guo[b] and Ya Li*[a]

Purpose: the aim of this study was to improve the stability and bioavailability of paeoniflorin (PF) by using nanoparticle encapsulation technology. *Methods*: paeoniflorin nanoparticles (PF NPs) were prepared with PLGA as the carrier using the compound emulsion method. The nanoparticles were characterised by using a Malvern laser particle sizer, transmission electron microscope (TEM), X-ray diffraction (XRD) analyser, and Fourier-transform infrared (FT-IR) spectrometry. The PF NPs were subjected to a series of stability investigations (such as for 4 °C storage stability, pH stability, and thermal stability), lyophilisation protection technology investigations, and *in vitro* release studies. Finally, the intestinal absorption properties of PF and PF NPs were studied by the *in situ* single-pass intestinal perfusion (SPIP) rat model, using the effective permeability coefficient (P_{eff}) and the absorption rate constant (K_a) as relevant indexes. *Results*: the prepared nanoparticles had a particle size of 105.0 nm with blue opalescent, rounded morphology, uniform size, good stability and slow release. We found that 4% alginate was the best lyoprotectant for the PF NPs. In the intestinal absorption experiments, P_{eff} was higher for the PF NPs group compared with the original PF material drug group in all intestinal segments ($P < 0.05$), and the absorption rate constant K_a increased with the increase in the drug concentration. *Conclusion*: the nanoparticles produced by this method have good stability and a slow-release effect; they can thus improve the absorption of PF in rat intestines, helping improve the stability and bioavailability of PF and enhancing its pharmacological effects.

Received 9th May 2024
Accepted 30th June 2024

DOI: 10.1039/d4ra03419h

rsc.li/rsc-advances

1. Introduction

Paeoniflorin (PF) is a water-soluble monoterpene glycoside, which is the main active ingredient of traditional Chinese medicine involving peony and red peony roots.[1] PF is a hygroscopic amorphous powder with a melting point of 196 °C. It is stable in acidic environments (pH of 2.0–6.0), but not in alkaline environments. It easily decomposes upon contact with heat.[2] Its molecular formula is $C_{23}H_{28}O_{11}$ with a molecular weight of 480.45 g mol^{-1}. Under normal use conditions, there is no obvious adverse reaction to the body.[3] In recent years, many studies have shown that PF has pharmacological effects, such as inhibiting platelet aggregation, thrombosis, anti-atherosclerosis, dilating coronary blood vessels, increasing coronary blood flow, and improving microcirculation,[4–7] and thus, it has been widely used in the research on the treatment of cardiovascular diseases.

However, due to its unstable physicochemical properties, it is susceptible to the influence of light, oxygen, heat, acid, and other changes in structure, along with poor intestinal absorption, causing its bioavailability to be only 3–4%,[8] which greatly impedes its clinical applications. Therefore, to promote the clinical application of PF by increasing its bioavailability *in vivo*, there is an urgent need to improve the stability and intestinal absorption properties of PF through some formulation techniques. There are many dosage forms, such as nanocrystals, microemulsions, liposomes, and microneedles, that can improve the stability and bioavailability of PF, but some of them have certain limitations. For instance, microemulsions require high solubility of drugs in the oil phase; phospholipid complexes require organic solvents and have complicated processes of preparation, and liposomes suffer from the problems of low drug-carrying capacity and poor stability.[9,10] Because of their internal dual channel structure and huge surface area of the membrane, nanoparticles can encapsulate various polar drugs, while featuring simple processes and good stability. Polylactic-*co*-glycolic acid (PLGA) is a commonly used carrier in nanoparticles, which is approved by the US FDA for clinical applications.[11] Due to its good biocompatibility and biodegradability; ability to solubilise, encapsulate, protect, and promote drug absorption; and slow release of drugs that prolongs the duration of action and enhances the stability of drugs, it has been widely used in the development of different

[a]*School of Pharmacy, Hunan University of Chinese Medicine, Changsha 410208, China. E-mail: 003872@hnucm.edu.cn*
[b]*School of Chinese Medicine, Hunan University of Chinese Medicine, Changsha 410208, China*

forms of drugs for the treatment of cardiovascular diseases.[12] Pu[13] prepared Salvianic acid A as a PLGA nanoparticle using PLGA as a carrier to find that PLGA nanoparticles can slow the release of the drug, prolong the duration of action, and increase the stability of the drug. Cao[14] loaded rapamycin with PLGA as a carrier and found that rapamycin PLGA nanoparticles increase the solubility of the drug, achieve long-lasting blood circulation, target atherosclerotic drug delivery, and significantly inhibit the development of atherosclerotic plaques. This indicates that PLGA nanoparticles can significantly change the oral bioavailability of rapamycin and enable it to perform better in its cardiovascular protective effects.

Polymeric nanoparticles have been widely used for drug delivery. Common preparation methods for them include nanodeposition, salting-out emulsification-diffusion, spontaneous emulsification-solvent diffusion, supercritical fluid technology, and emulsification-solvent evaporation.[15] Emulsification-solvent evaporation method is a commonly used technique for the preparation of PLGA polymer nanoparticles. The polymer is dissolved in an aqueous organic solvent, which is stabilized at the interface by a surfactant in a spherical shape. During solvent evaporation, the solvent diffuses into the continuous aqueous phase and forms nanoparticles after desolvation. The emulsification-solvent evaporation method is divided into single-emulsion and complex-emulsion methods, which are suitable for lipophilic and water-soluble drugs, respectively.[16]

PF is a water-soluble drug that can easily diffuse into the aqueous phase during preparation, resulting in a low encapsulation rate, and thus, the compound emulsion method was used for preparation. In other words, PF was first dissolved in water and then dispersed into an organic solvent containing the polymer to form a W/O-type colostrum. Finally, the colostrum was dispersed into the aqueous phase to form a W/O/W-type compound emulsion, and nanoparticles were formed after the solvent evaporated.

In recent years, researchers have studied the application of nanoparticles as a route of drug delivery and compared them with other such routes; the oral route is still the most widely preferred method of drug delivery due to its convenience, low cost, and high patient compliance.[17] Drugs taken orally are mainly absorbed in the intestinal tract, and thus, the intestinal absorption characteristics of drugs are among the determinative factors for the efficacy of orally administered drugs.[18] Oral bioavailability of drugs is primarily related to drug stability and absorption in the gut. Poor oral bioavailability of PF is due to its low lipophilicity, poor intestinal permeability, p-glycoprotein-mediated efflux, and hydrolysis of large amounts of glycosides in the gut.[19,20] Therefore, it was investigated whether PF NPs could improve the stability of PF and enhance the intestinal absorption of the drug by an *in situ* single-pass intestinal perfusion model.

Therefore, in this study, PF was combined with a PLGA carrier to prepare a new dosage form of PF that was characterised by a series of techniques for nanoparticles. The stability of PF NPs was investigated, including storage stability at 4 °C, pH stability, and thermal stability. In addition, lyophilization protection techniques and *in vitro* release studies were performed. Finally, the intestinal absorption properties of traditional PF and PF NPs were studied and evaluated by *in situ* single-pass intestinal perfusion experiments using important indexes, effective permeability coefficient (P_{eff}) and absorption rate constant (K_a). This study will help improve the stability and bioavailability of PF, and thus, better exert its pharmacological effects.

2. Materials and methods

2.1 Materials

Paeoniflorin (purity ≥98%) was purchased from Tongze Biotechnology Co., Ltd (Xi'an, China). PLGA (molecular weight: 30 000) was purchased from Daigang Biotechnology Co. Ltd (Jinan, China). Methanol, pepsin, $CaCl_2$, NaCl, KCl, NaH_2PO_4, $NaHCO_3$, and $MgCl_2$ were purchased from Sinopharmaceutical Reagent Co., Ltd (Shanghai, China). Trypsin was purchased from Feijing Biotechnology Co., Ltd (Fuzhou, China), and all other chemicals were of analytical or HPLC grade.

2.2 Animals

Healthy sprague-dawley rats (SD), aged 8 weeks with a body weight range of 230–270 g (equal number of male and female), were purchased from Slake Jinda Animal Co. Ltd (Hunan, China; laboratory animal production license No.: SCXK (Xiang) 2019-0004). The rats were housed and maintained at the Animal Experimental Center of Hunan University of Chinese Medicine. The experiments were carried out in accordance with the Regulations on the Management of Laboratory Animals in Hunan Province and were approved by the Ethics Committee of Animal Experimentation of Hunan University of Chinese Medicine (Ethics Approval No.: LL2023051902).

2.3 Preparation of nanoparticles

The prescribed amount of PF was precisely weighed and dissolved into an appropriate amount of distilled water as the internal aqueous phase. Another prescribed amount of PLGA was dissolved in 1.5 mL of acetone as the oil phase. The internal aqueous phase was injected into the oil phase and sonicated at 100 W for 10 seconds to form colostrum. Colostrum was then slowly injected into 5 mL of 0.4% poloxamer 188, and sonicated at 100 W for 2 minutes to form the multiple emulsion, which was injected into 10 mL of 0.1% poloxamer 188, stirred with a magnetic stirrer until acetone completely evaporated. The products were then placed in an ultrasonic cell crusher for ultrasonic disruption in an ice bath for 5 minutes and then passed through a 0.22 μm microporous filter membrane to yield the final product.

2.4 Determination of PF content by HPLC

Chromatographic conditions: the Hyperdil BDS C_{18} column (4.6 mm × 200 mm, 5 μm) was used with chromatographic acetonitrile as the organic phase (A) and 0.1% phosphoric acid solution as the aqueous phase (B). The ratio of A to B was 20 : 80. The injection volume was 10 μL; the detection wavelength was

230 nm, and the temperature of the column was 30 °C. Under such chromatographic conditions, the PF control, PF NPs, and the blank nanoparticle solutions were investigated for their specificity. The PF control series of 2.5, 5, 10, 20, 40, and 100 μg mL^{-1} were prepared by dilution with 70% methanol. Linear regression was performed with the peak area of PF as the vertical coordinate (Y), and the actual concentration as the horizontal coordinate (X). The methodology was evaluated based on its precision, stability, and recovery of spiked material to ensure the stability and reliability of the established method for the determination of PF.

2.5 Characterisation of nanoparticles

2.5.1 Determination of the nanoparticle encapsulation rate. First, 2 mL of PF NPs were taken in a beaker and 100 mL of pure water was added; another 5 mL of pure water was placed in a dialysis bag that was tied at both ends and placed in the beaker containing the nanoparticle solution. Magnetic stirring was performed at a constant temperature of 100 rpm. After 6 h of dialysis, 1 mL of the solution was aspirated from the dialysis bag, passed through a 0.22 μm filter membrane, and the amount of free drug was determined in pipetted precisely 1.0 mL of the PF NPs test sample by HPLC. Methanol was added to break the emulsion by ultrasonication, and the total amount of the drug was calculated after determining the encapsulation rate with the following equation:

$$\text{Encapsulation rate (\%)} = (\text{total drug amount} - \text{free drug amount})/\text{total drug amount} \times 100\%$$

2.5.2 Determination of the nanoparticle drug loading capacity. PF NPs suspension was placed in a freeze dryer and dried completely. The lyophilized powder was weighed accurately and its net mass was recorded. Finally, the total amount of drug in the lyophilized powder was determined, and the drug loading was calculated:

$$\text{Drug loading} = \text{total drug amount/net mass of lyophilized powder}$$

2.5.3 Determination of particle size and Zeta potential. The average particle size, PDI, and Zeta potential of the PF NPs were determined using a Malvern laser particle sizer on 1 mL of nanoparticle suspension diluted with distilled water.

2.5.4 Morphological observation of PF NPs. Ten microliters of PF NPs were added dropwise and precipitated on a copper grid for 1 minutes, followed by the addition of 10 μL of uranyl acetate dihydrate dropwise. The contents on the grid were then dried and imaged by electron microscopy detection at 80–120 kV.

2.5.5 Fourier infrared spectroscopy (FT-IR) analysis of PF NPs. Infrared spectra were acquired for samples of PF (A), blank NPs (B), and PF NPs (C) by an infrared spectrometer across a wave number range of 4000 to 400 cm^{-1}.

2.5.6 X-ray diffraction (XRD) analysis of PF NPs. Dried powders of PF (A), blank NPs (B), and PF NPs (C) samples were placed on slides and scanned at 2° min^{-1} in the range of 5–90° under a Cu-Kα-ray light source using an X-ray diffractometer.

2.6 Examination of nanoparticle stability

2.6.1 Storage stability. A suspension of PF NPs was placed in a refrigerator at 4 °C, and samples were collected at 0, 3, 7, 14, and 30 days, respectively, to determine the particle size, PDI, and Zeta potentials. The stability of the nanoparticles was investigated during storage of the formulations under 4 °C conditions.

2.6.2 pH stability. 10 mL of PF NPs were adjusted using hydrochloric acid and sodium hydroxide solutions to obtain different pH values (3.0, 5.0, 7.0, and 9.0). Their particle size, Zeta potential, and PF retention were determined. The PF content before pH treatment is considered to be 100%.[21]

$$\text{Retention (\%)} = C/C_0 \times 100\%.$$

Note: C indicates PF content after different pH treatments; C_0 indicates PF content before no treatment.

2.6.3 Thermal stability. The samples were heat-treated at 60, 80, and 100 °C for 15, 30, and 60 minutes, respectively. Particle size, Zeta potential, and PF retention were measured for each sample after heating, and the PF content before heat treatment was considered to be 100%. The formula for calculating the retention rate is the same as in "Section 2.6.2".[22]

2.6.4 Gastrointestinal stability simulation experiment. To simulate gastric digestion, simulated gastric fluid was prepared according to the Chinese Pharmacopoeia: 16.4 mL of dilute hydrochloric acid was added to ~800 mL of water with 20 g of pepsin, shaken well, and then diluted with distilled water to a final volume of 1 L. PF was mixed with simulated gastric fluid in a ratio of 1 : 3 in a tube (pH = 1.5) and then shaken well for 2 hours at 37 °C. To simulate the intestinal phase, 30 mL of the digested sample was collected at the end of the gastric digestion phase and transferred to another tube. Four millilitres of a PBS buffer (pH = 7.0) containing 0.34 g of potassium dihydrogen phosphate and 0.5 g of trypsin PBS solution were prepared and added to the digested samples. The pH of the mixture was then adjusted to 6.8. At the end of each stage, particle size, PDI, and nanoparticle digestion were observed and recorded.[23]

2.7 Study of *in vitro* nanoparticle release

2 mL each of PF and PF NPs solution were added to a dialysis bag and sealed. Three different dialysis media, 100 mL of PBS (pH = 7.4), simulated gastric fluid, and simulated intestinal fluid, were prepared. The dialysis bags were placed into each dialysis medium and dynamically dialyzed at a constant temperature of 37 °C in a water bath at a speed of 100 rpm. At 0.25, 0.5, 1, 2, 3, 4, 5, 6, 8, 10, 12, and 24 hours, 1 mL of the dialysis medium was aspirated, and the same volume of blank medium was added to make up for volume loss; the solution was taken out and passed through a 0.22 μm filter membrane, and the concentration of PF in the releasing medium was determined by HPLC. The cumulative release rate was calculated and plotted as a curve.

$$E_r = \frac{V_e \sum_{1}^{n-1} C_i + V_0 C_n}{m_{drug}}$$

where E_r indicates cumulative drug release; V_e indicates displacement volume of the dialysis medium; V_0 indicates the total volume of release medium; C_i indicates the concentration of release solution at the ith displacement sampling; m_{drug} indicates the total mass of drug contained in the nanoparticles; n indicates the number of times of displacement of dialysis medium.

2.8 Screening of lyoprotectants

2 mL of each PF NPs solution was taken in a vial, and sucrose, glucose, lactose, alginate, and mannitol were added as lyoprotectants; a blank control group was also set up. The samples were first placed in a −20 °C refrigerator to freeze for 6 hours, followed by immediate transfer to a −40 °C refrigerator to freeze for 12 hours; finally, the samples were placed in a vacuum freeze dryer to freeze until they were completely dry to obtain a lyophilised powder. The appearance morphology (0–10 points), redispersibility (0–10 points), redispersibility index (RI; RI = particle size after re-dissolution/particle size of nanoparticle solution before freeze-drying), and polydispersity index (PDI) after re-dissolution were used as evaluation indexes to preferably select the optimal lyoprotectant.

2.9 Characterisation of intestinal absorption

2.9.1 Preparation of solutions. We dissolved 0.37 g of $CaCl_2$ in a small amount of distilled water to obtain a $CaCl_2$ aqueous solution; 7.8 g of NaCl, 0.35 g of KCl, 0.32 g of NaH_2PO_4, 1.37 g of $NaHCO_3$, and 0.02 g of $MgCl_2$ were dissolved in an appropriate amount of distilled water. Drop by drop, the latter solutions were added to the $CaCl_2$ aqueous solutions, with the addition of glucose and the volume was adjusted to 1000 mL with a pH of 7.4, which yielded the Krebs–Ringer (K–R) solution.[24] The blank K–R solution was subjected to a single-pass intestinal perfusion method based on *in situ* processes in rats for 150 minutes; the effluent was collected. The PF and PF NPs were weighed precisely and dissolved in the K–R solution to obtain the 50 μg mL^{-1} PF solution for high concentration PF and PF NPs enteric perfusion test solution. The solution was diluted using the K–R solution to obtain the 50, 25, 12.5 μg mL^{-1} PF solutions with high, medium, and low concentrations for the enteric perfusion test.

2.9.2 *In situ* single-pass intestinal perfusion experiments in rats. Healthy SD rats were fasted for 12 hours with a normal water intake. The rats were injected intraperitoneally with 5% pentobarbital sodium at a dose of 45 mg kg^{-1}. After anaesthesia, the rats were immobilized on the operating table and their body temperature was maintained. Approximately 2–3 cm long sections were cut in the midline of the abdomen, the choledoch was ligated, and intestinal segments were slowly separated for examination (duodenum, jejunum, ileum, and colon). The length of each segment was ~10 cm. Both ends of the segments were incised. Glass tubes were inserted and ligated, followed by fixation with surgical wires. The intestinal contents were rinsed out slowly with preheated saline at 37 °C, and then the saline was emptied with air. The proximal glass tube was connected to a peristaltic pump and the wound was covered with saline moistened gauze to keep the bowel moist. The drug-containing intestinal perfusate was perfused into the intestinal segment at a flow rate of 1.0 mL min^{-1} for 10 minutes. The flow rate was then adjusted to 0.3 mL min^{-1}, and equilibrated for 30 minutes. After 30 minutes, the inlet was replaced with a centrifuge tube containing a known mass of drug-containing perfusate. The outlet was replaced with a blank centrifuge tube for collection of effluent, and the two were changed together once every 15 minutes; the switch was performed 10 times.[25] At the end of the experiment, the rats were executed by cervical dislocation, and the length of the intestinal segment (L), and the radius of the intestinal segment's cross-section (r) were measured.

2.9.3 Sample handling and calculation of correlation constants. The effluent was collected in a 5 mL centrifuge tube and centrifuged at 10 000 rpm for 15 minutes at 4 °C in a freezing centrifuge. The supernatant was removed, passed through a 0.22 μm filter membrane, and stored in a liquid-phase vial at 4 °C in the refrigerator before measurements.

The effective permeability coefficient (P_{eff}) and absorption rate constant (K_a) are important indicators for evaluating drug absorption, where P_{eff} refers to the speed and extent of drug molecules passing through the skin or mucous membranes, and K_a is the degree of rapidity with which the drug absorbs in the body. They were calculated using the gravimetric method represented in the following equation. Where ρ_{in} and ρ_{out} indicate the mass concentration of inlet and outlet intestinal perfusates (μg mL^{-1}), respectively; V_{in} and V_{out} indicate the volume of perfusate infused into and collected from the intestines (mL), respectively. L and r indicate the length of the intestinal segment and the cross-sectional radius of the rat intestine (cm), respectively. Q indicates the flow rate of the intestinal perfusate (min mL^{-1}). The density of the perfusate was assumed to be approximately 1.0 g mL^{-1}.

$$K_a = \left(1 - \frac{\rho_{out}}{\rho_{in}} \times \frac{V_{out}}{V_{in}}\right) \times \frac{Q}{\pi r^2 l}$$

$$P_{eff} = \frac{-Q \ln\left(\frac{\rho_{out}}{\rho_{in}} \times \frac{V_{out}}{V_{in}}\right)}{2\pi r}$$

2.10 Statistical analyses

SPSS 25.0 software was used for statistical analysis. All measurements are expressed as mean ± standard deviation ($\bar{x} \pm s$). The independent samples t-test was used for comparison between groups, where $P < 0.05$ was used to indicate a statistically significant difference.

3. Results

3.1 Methodological investigations for the determination of PF content

The results of the specificity showed that the control and test solutions presented characteristic peaks at the same relative

retention time, while the blank solution did not, indicating that the blank nanoparticles did not interfere with the determination of paeoniflorin. The regression equation for the actual concentration of PF (X) and the peak area (Y) was $Y = 12.486X - 5.1042$, $r = 0.9999$. This indicated that PF had a good linear relationship in the mass concentration range of 6.5–100 μg mL^{-1}. The results of methodological investigations showed that the RSD% of precision and stability of each concentration group was below 2%, and the recoveries of spiked samples were in the range of 97.02–98.51%, indicating that the established method for the determination of PF content was reliable.

3.2 Nanoparticle characterisation

The encapsulation rate of PF NPs was measured to be 45.49%, and the drug loading was 4.52%. The laser particle size analyser measured the average particle size of PF NPs as 105.0 nm (Fig. 1A), the PDI was 0.182, and the Zeta potential was −22.9 mV (Fig. 1B). The sample solution of PF NPs is shown in Fig. 1D, and images from its transmission electron microscopy are in Fig. 1C. They showed that the PF NPs presented a blue milky light, and the nanoparticles were rounded and homogeneous. The X-ray diffraction of PF NPs was analysed to show that the crystal structure changed after PF was incorporated into the nanoparticles because it exhibited the same characteristic diffraction peaks as the material (Fig. 1E), indicating that PF was successfully encapsulated by the PLGA material. The IR spectrum shown in Fig. 1F has the stretching vibration peaks of –OH and C–O–C of PF at 3461.60 and 1282.91 cm^{-1}, respectively, while the peaks of PF NPs are weakened, and show the same features as those of the materials. The characteristic peak from the monosubstitution of the benzene ring of PF appears at 715.46 cm^{-1}, and it disappears in the case of PF NPs, indicating their successful preparation.

3.3 Nanoparticle stability

3.3.1 Storage stability. The results of nanoparticle stability upon placement at 4 °C are shown in Table 1. They indicate that the values of particle size, PDI, and Zeta potential of PF NPs underwent small changes compared to day 0, upon placement at 4 °C for 30 d, indicating that the suspension of PF NPs was well-stabilized at 4 °C.

Table 1 Storage stability of PF NPs at 4 °C ($\bar{x} \pm s$, $n = 3$)

Time at 4 °C d^{-1}	Particle size (nm)	PDI	Zeta potential (mV)
0	125.4 ± 0.660	0.114 ± 0.004	−22.9 ± 0.411
3	127.8 ± 1.461	0.118 ± 0.005	−21.8 ± 1.157
7	126.6 ± 0.873	0.115 ± 0.004	−22.7 ± 1.349
14	126.3 ± 1.891	0.119 ± 0.002	−20.1 ± 0.249
30	127.1 ± 1.676	0.122 ± 0.009	−20.1 ± 0.045

3.3.2 pH stability and thermal stability. The results of pH stability and thermal stability of the PF NPs are shown in Fig. 2, and the particle size of PF NPs is shown in Fig. 2A. Neither of these parameters changed significantly with increasing pH, indicating that the nanoparticles were stable under pH 3–9. The absolute value of the Zeta potential of PF NPs increased gradually with increasing pH, while remaining negatively charged. The change in the Zeta potential may be due to increasing OH^- content at higher pH values. From Fig. 2B, it can be seen that PF and PF NPs can be retained together above 95% at pH 3–5, while the retention gradually decreases with increasing pH, indicating that PF is stable under acidic conditions and unstable under alkaline conditions. However, the retention of PF NPs was significantly higher than that of PF above pH 5 ($P < 0.05$), indicating that after PLGA encapsulation, PF could be protected from decomposition and have enhanced stability.

Fig. 2C shows the changes in particle size and Zeta potential of PF NPs after treatment at 60, 80, and 100 °C. From the results, it can be seen that there is no significant change in the particle size and Zeta potential of PF NPs after treatment at different times and temperatures. This observation indicates that PF NPs have good thermal stability. As can be seen in Fig. 2D, the retention

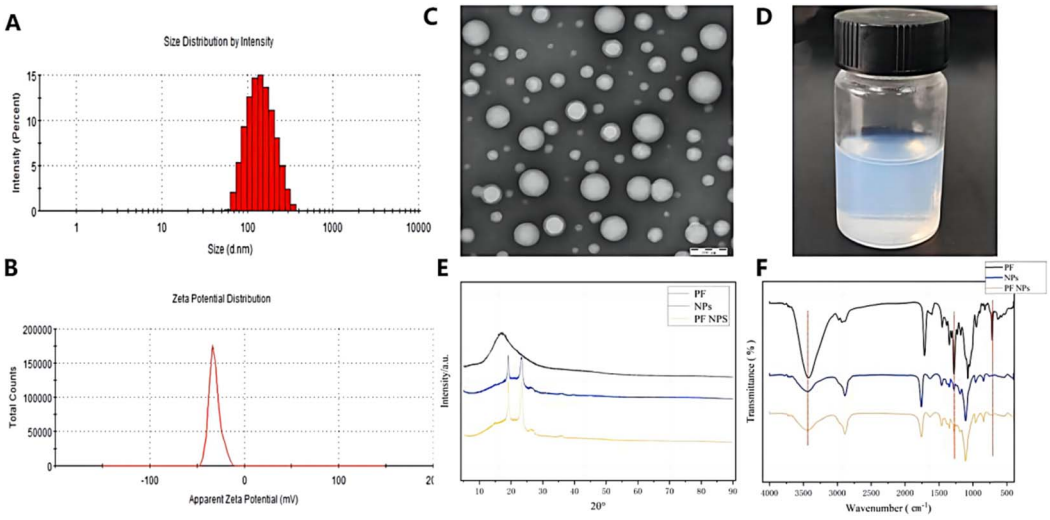

Fig. 1 Characterisation of PF NPs with the particle size distribution graph (A), Zeta potential graph (B), transmission electron microscopy image (C), sample map of nanoparticles (D), XRD graph (E), FT-IR graph (F).

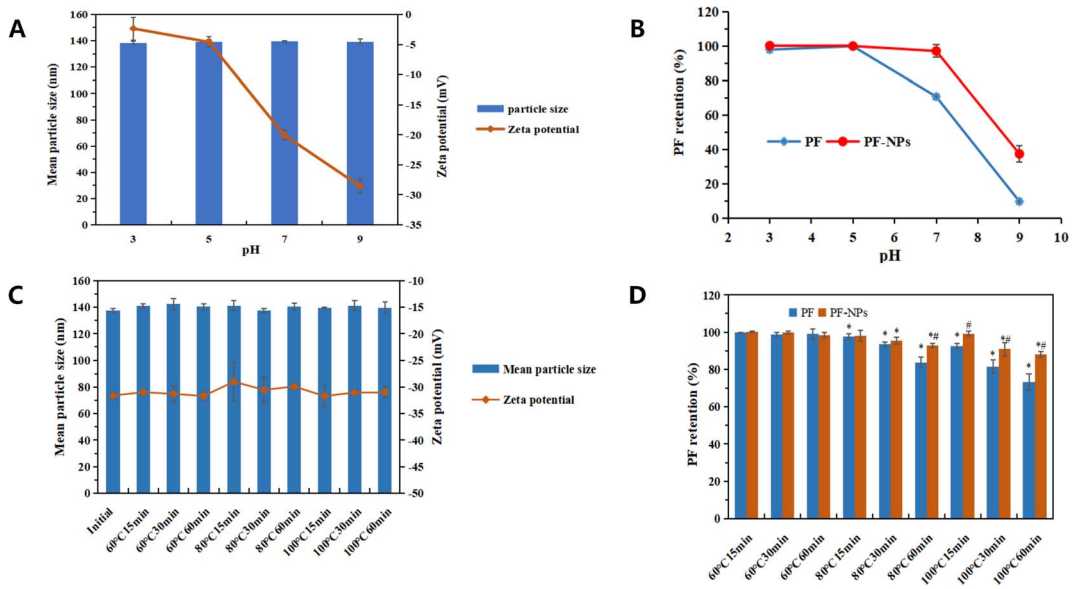

Fig. 2 (A) Changes in particle size and Zeta potential of PF NPs at different pH, (B) retention of PF and PF NPs at different pH, (C) changes in particle size and Zeta potential of PF NPs after different heating treatments, (D) retention of PF and PF NPs after different heating treatments ($\bar{x} \pm s$, $n = 3$), compared with the initial retention (*$P < 0.05$, the #$P < 0.05$) and under the same heating conditions.

rates of PF and PF NPs did not change significantly after being heated to 60 °C, but decreased gradually with time at 80 °C and 100 °C. However, the retention rates of PF NPs were higher than those of PF after 60 minutes of heating at 80 °C and 15, 30, and 60 minutes of heating at 100 °C, which indicated that PF had enhanced thermal stability after it was wrapped in nanoparticles.

3.3.3 Modelling gastrointestinal stability. After simulated gastrointestinal peristaltic digestion, the stability of PF NPs was investigated, and the results are shown in Fig. 3. As shown in Fig. 3A, the particle size and PDI of PF NPs did not show obvious changes in different digestion stages. Fig. 3B shows the appearance and morphology of nanoparticles after simulated gastrointestinal digestion for 1, 2, 4, and 6 hours. During the simulated dynamic digestion process, the PF NPs were clarified in gastric and intestinal fluids without obvious aggregation and sedimentation, indicating that the PF NPs were stable in the gastrointestinal tract.

3.4 *In vitro* release

Drug release curves were plotted as a function of dialysis time, *i.e.*, the horizontal coordinate was time, and the cumulative drug release rate was the vertical coordinate, as shown in Fig. 4. Fig. 4A shows the release curves for PF and PF NPs in PBS. The cumulative release rate did not differ much during the early stages, which may be because some free drugs still existed in the nanoparticle suspension. During the later stages, PF was released completely at 10 hours, while the prepared PF NPs were still being released slowly at 24 hours, indicating that the drug could be released slowly in physiological media after being wrapped in nanoparticles. This delay in release is due to the blocking effect of PLGA on the drug, and the same slow release effect is shown in artificial gastric fluid (Fig. 4B) and artificial intestinal fluid (Fig. 4C). The release rate of PF NPs in physiological media was in the order: artificial intestinal fluid > artificial gastric fluid > PBS.

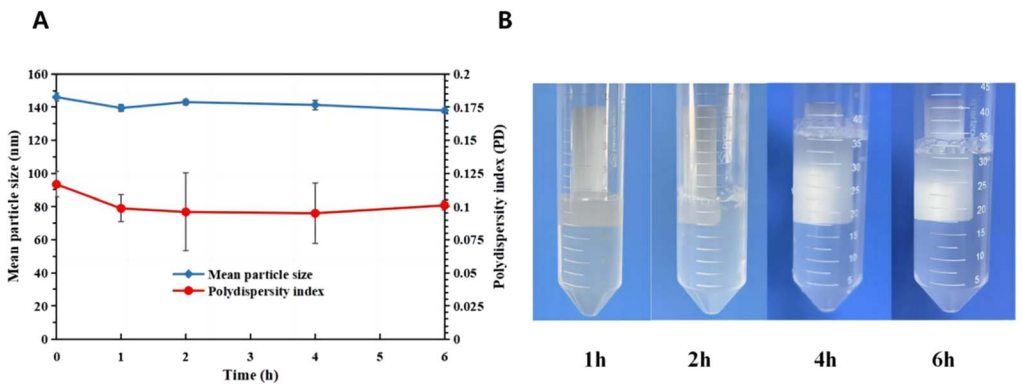

Fig. 3 Changes in the particle size and PDI during simulated gastrointestinal digestion of PF NPs (A) and appearance (B).

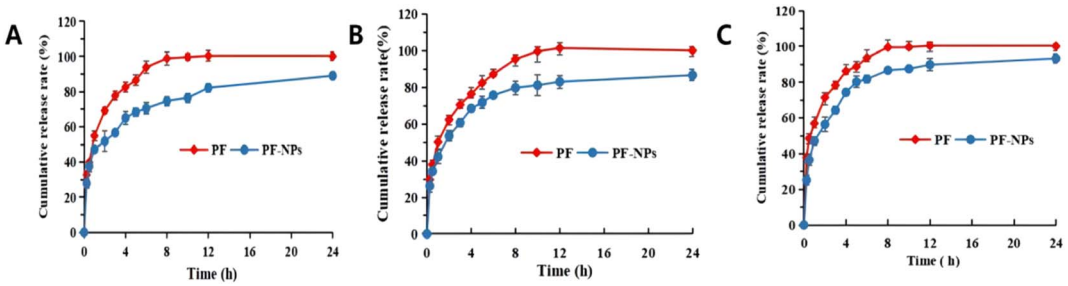

Fig. 4 *In vitro* release profiles of PF and PF NPs in different physiological media ($\bar{x} \pm s$, $n = 3$), (A) PBS, (B) simulated gastric fluid, (C) simulated intestinal fluid.

3.5 Lyophilised protectant screening

To minimize or avoid irreversible aggregation during freeze-drying, a lyoprotectant can be added to the suspension solution being frozen. In Table 2, it can be seen that after lyophilization of PF NPs without lyoprotectant, most of them apparently collapsed, *i.e.*, the color was not uniform anymore; the re-dispersibility was poor, and the particle size increased. As shown in Fig. 5, the appearance of the sample containing 3% alginate lyoprotectant was significantly better; the lyophilized powder was full and smooth with consistent color, no wrinkling and collapse; the change in the particle size was small, and the PDI and Zeta potentials were better than those of the other samples that contained different concentrations of lyoprotectants. Therefore, 3% alginate can be chosen as the lyoprotectant for PF NPs.

Fig. 5 Appearance and morphology of PF NPs samples containing 3% of alginate lyoprotectant after lyophilization.

3.6 Nanoparticle intestinal absorption properties

Different concentrations of PF and PF NPs were absorbed to a certain extent in the duodenum, jejunum, ileum, and colon. The results of the P_{eff} calculation are shown in Fig. 6, and the results of the K_a calculation are summarised in Table 3. The results showed that, except for the high concentration in the colon, the P_{eff} of the PF NPs group was significantly higher than that of the group with the same concentration of PF in all the segments of the intestines ($P < 0.05$). In this regard, the duodenum was more obvious. The mean P_{eff} at all the concentrations and K_a increased with an increase in the mass concentration of PF, suggesting that the main mode of transport of PF into the body circulation may be passive transport.

Table 2 Results of lyophilised protectant screening ($\bar{x} \pm s$, $n = 3$)

Lyophilisate	Concentration (%)	Surface	Redispersibility	RI	PDI	Zeta potential (mV)
Blank	0	3	3	1.65	0.267 ± 0.007	−17.3 ± 0.46
Glucose	1	0	10	1.17	0.219 ± 0.004	−17.4 ± 0.15
	3	0	10	1.95	0.227 ± 0.02	−15.2 ± 0.83
	5	3	10	3.22	0.278 ± 0.004	−12.7 ± 0.36
Alginate	1	3	10	1.12	0.221 ± 0.025	−15.4 ± 0.25
	3	10	10	1.05	0.216 ± 0.002	−18.4 ± 0.26
	5	10	7	1.43	0.248 ± 0.043	−13.2 ± 0.85
Lactose	1	7	3	2.27	0.259 ± 0.019	−15.7 ± 0.64
	3	7	0	2.43	0.368 ± 0.038	−14.3 ± 1.31
	5	10	0	2.45	0.330 ± 0.028	−14.7 ± 0.09
Fructose	1	3	7	1.16	0.197 ± 0.010	−16.9 ± 0.42
	3	3	10	1.39	0.203 ± 0.016	−18.7 ± 0.49
	5	3	10	2.83	0.170 ± 0.012	−18.7 ± 0.55
Mannitol	1	0	7	2.16	0.275 ± 0.023	−18.2 ± 0.31
	3	3	7	4.45	0.321 ± 0.017	−19.1 ± 1.42
	5	7	3	4.07	0.304 ± 0.059	16.0 ± 0.70

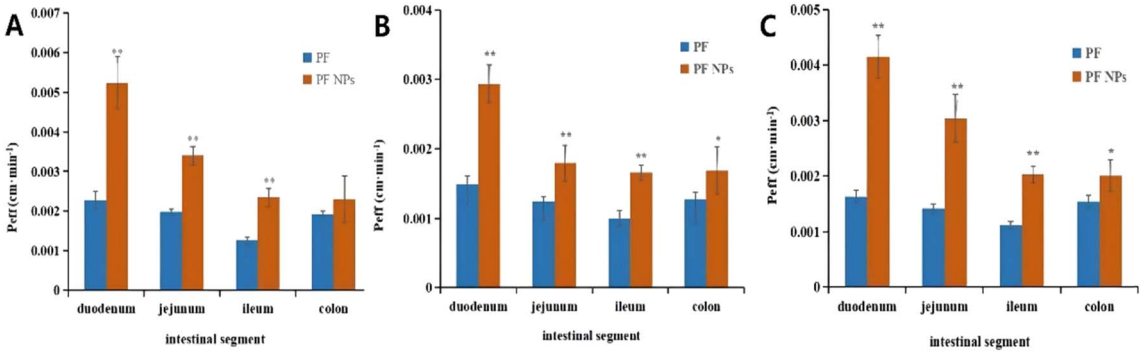

Fig. 6 Effective permeability coefficients (P_{eff}) for different mass concentrations of PF and PF NPs in different intestinal segments. Comparison is presented with the group of PF with the same mass concentration and intestinal segments ($\bar{x} \pm s$, $n = 3$), *$P < 0.05$, **$P < 0.01$, (A) 50 μg mL^{-1}, (B) 25 μg mL^{-1}, (C) 12.5 μg mL^{-1}.

Table 3 Absorption rate constants for PF and PF NPs in different intestinal segments K_a/min^{-1}, $\times 10^{-2}$, ($\bar{x} \pm s$, $n = 6$)

Intestinal segment	Concentration (μg mL^{-1})	PF	PF NPs
Duodenum	50	3.46 ± 0.46^{b}	$5.08 \pm 0.74^{a,b}$
	25	2.30 ± 0.38	$4.26 \pm 0.69^{a,b}$
	12.5	2.26 ± 0.35	2.80 ± 0.57
Jejunum	50	2.88 ± 0.39^{b}	3.16 ± 0.48^{b}
	25	2.12 ± 0.35	$3.12 \pm 0.59^{a,b}$
	12.5	1.79 ± 0.25	1.72 ± 0.27
Ileum	50	1.60 ± 0.21	$2.52 \pm 0.25^{a,b}$
	25	1.78 ± 0.19^{b}	1.76 ± 0.22^{b}
	12.5	1.47 ± 0.25	1.51 ± 0.14
Colon	50	2.22 ± 0.13^{b}	2.53 ± 0.74^{b}
	25	2.02 ± 0.03^{b}	2.04 ± 0.31
	12.5	1.45 ± 0.14	1.78 ± 0.44

[a] Indicates $P < 0.05$ for comparison with the group having the same dose of PF. [b] Indicates $P < 0.05$ for comparison with the low-concentration group and the same gut segment.

4. Summary and discussion

In the present work, PF NPs were prepared using PLGA as a carrier using a complex emulsion method. The resulting PF NPs had an average particle size of 122.0 ± 2.627 nm, an encapsulation rate of 45.49%, and a drug loading capacity of 4.52% with a regular morphology and uniform size. The results of pH stability and thermal stability experiments showed that the nanoparticles enhanced the stability of PF. Furthermore, the nanoparticles were not destroyed during the simulated gastrointestinal digestion process, indicating that the prepared nanoparticles were stable and reliable. Different concentrations of various lyoprotectants were investigated, and it was found that with 3% alginate as lyoprotectant, the dried lyophilized powder product was full and smooth, with consistent colour, no wrinkles, and good re-dispersibility. The particle size was small after re-solubilization, which effectively prevented the PF NPs from aggregating. The *in vitro* release results in different physiological media showed that the PF NPs could release the drug slowly and prolong its action time. *In situ* single-pass intestinal perfusion study for the intestinal absorption of PF showed that PF and PF NPs have a certain degree of absorption in the rat intestinal segments; the best absorption occurred in the duodenum. The incorporation of PF into the nanoparticles can significantly improve the absorption in the intestinal tract. For the high concentration group in the duodenum, jejunum, ileum, and colon, P_{eff} increased by 2.3, 1.7, 1.9, and 1.2 times, respectively. K_a in the PF NPs group increased with an increase in the PF mass concentration, indicating that the main mode of transport of PF into the body circulation may be passive transport.

Currently, intestinal absorption models for oral nanoparticle drug delivery systems can be categorized as *in vitro*, *in situ*, and *in vivo*.[26] The *in vitro* model includes dialysis bags, intestinal capsular exstrophy, and cell culture models. The *in situ* methods include enteral perfusion and intestinal loop methods, and the *in vivo* method includes blood/urine drug concentration methods. The *in vitro* experiments are simple and easy to perform, but they do not adequately reflect the actual absorption of nanoparticles *in vivo*. The *in vivo* method can truly reflect the absorption of nanoparticle-conjugated drugs in the intestinal tract, but it may be affected by physical and physiological factors, and thus, it cannot specifically reflect the absorption in the intestinal tract. The *in vivo* metabolism of individual experimental animals varies greatly, and thus, there are more uncertainties in the experimental complexity. Therefore, this method is not suitable for rapid screening and large-scale evaluation in early drug development. The *in situ* single-pass intestinal perfusion model is currently the most widely used model for studying the intestinal absorption of orally administered drugs. It can simulate intestinal peristalsis at a low flow rate, reduce the damage to the intestinal wall, and is one of the models recognized by the US FDA for drug absorption studies.[27]

According to the experimental results, the main absorption site of PF is located in the small intestine, mainly due to the large epithelial surface area of this part of the intestine. The upper intestinal mucosa has many circular folds that can increase the surface area of the small intestinal mucosa. There are abundant small intestinal villi, whose stretching and waving

can promote the flow of the capillary network and lymphatic fluid, facilitating the absorption of the drug.[28] The nanoparticles can significantly improve the intestinal absorption of PF and help overcome the problems of poor oral absorption and low bioavailability, which may be attributed to the fact that the encapsulation of the drug by PLGA can reduce the exocytosis of PF by glycoproteins and increase its lipid solubility, enabling it to easily pass through the lipid layer, and thus, be taken up by the intestinal mucosa for transport.[29] However, its absorption mechanism needs to be further investigated. Subsequent studies on the absorption mechanism of PF NPs and their *in vivo* pharmacokinetics will be carried out to clarify the absorption mechanism and *in vivo* absorption, which will lay the foundation for the development of PF NPs formulations.

Author contributions

Yifei Xiao designed the experimental methods, processed the data, and drafted the manuscript. Qidong Wei and Lixin Du designed the experimental methods, processed the data, and conducted the experimental work. Zhihua Guo conducted research and data processing. Ya Li contributed to experimental design, manuscript drafting, and publication.

Conflicts of interest

The authors declare that the research was conducted in the absence of any commercial or financial relationships that could be construed as a potential conflict of interest.

Acknowledgements

This research was funded by The National Natural Science Foundation of China (82174343), the Key Discipline Project on Chinese Pharmacology of Hunan University of Chinese Medicine (202302), the Scientific Research Topics of Hunan Provincial Health and Wellness Commission (D202303017861), the Hunan University of Chinese Medicine Graduate Innovation Project (2022CX78), and the Postgraduate Scientific Research Innovation Project of Hunan Province (CX20230830).

References

1 F. Jiao, K. Varghese, S. Wang, *et al.*, Recent insights into the protective mechanisms of paeoniflorin in neurological, cardiovascular, and renal diseases, *J. Cardiovasc. Pharmacol.*, 2021, **77**(6), 728–734.
2 X. Yang, X. Li, Y. Zhu, *et al.*, Paeoniflorin upregulates mitochondrial thioredoxin of schwann cells to improve diabetic peripheral neuropathy indicated by 4D label-free quantitative proteomics, *Oxid. Med. Cell. Longev.*, 2022, **2022**, 4775645.
3 B. Bao, Y. Zhao, H. Gong, *et al.*, Quantification of paeoniflorin by fully validated LC-MS/MS method: its application to pharmacokinetic interaction between paeoniflorin and verapamil, *Molecules*, 2022, **27**(23), 8337.
4 X. Li, C. Sun, J. Zhang, *et al.*, Protective effects of paeoniflorin on cardiovascular diseases: a pharmacological and mechanistic overview, *Front. Pharmacol.*, 2023, **14**, 1122969.
5 W. Man, C. Wang, J. Wang, *et al.*, Promoting reverse cholesterol transport contributes to the amelioration of atherosclerosis by paeoniflorin, *Eur. J. Pharmacol.*, 2023, **961**, 176137.
6 F. Wu, B. Ye, X. Wu, *et al.*, Paeoniflorin on rat myocardial ischemia reperfusion injury of protection and mechanism research, *Pharmacology*, 2020, **105**(5–6), 281–288.
7 C. Shen, B. Shen, J. Zhu, *et al.*, Glycyrrhizic acid-based self-assembled micelles for improving oral bioavailability of paeoniflorin, *Drug Dev. Ind. Pharm.*, 2021, **47**(2), 207–214.
8 D. Wang, F. Yang, W. Shang, *et al.*, Paeoniflorin-loaded pH-sensitive liposomes alleviate synovial inflammation by altering macrophage polarity *via* STAT signaling, *Int. Immunopharmacol.*, 2021, **101**(Pt A), 108310.
9 C. Wu, B. Li, Y. Zhang, *et al.*, Intranasal delivery of paeoniflorin nanocrystals for brain targeting, *Asian J. Pharm. Sci.*, 2020, **15**(3), 326–335.
10 L. Zeng, S. Qiong, Y. Tang, *et al.*, Preparation of loaded paeoniflorin-polybutylcyanoacrylate microspheres and its sustained release performance *in vitro*, *Chin. J. Tradit. Med. Sci. Technol.*, 2022, **29**(03), 387–389.
11 P. Rafiei and A. Haddadi, Docetaxel-loaded PLGA and PLGA-PEG nanoparticles for intravenous application: pharmacokinetics and biodistribution profile, *Int. J. Nanomed.*, 2017, **12**, 935–947.
12 Z. Feng, S. Peng, Z. Wu, *et al.*, Ramulus mori polysaccharide-loaded PLGA nanoparticles and their anti inflammatory effects *in vivo*, *Int. J. Biol. Macromol.*, 2021, **182**, 2024–2036.
13 L. Pu, H. Yu, J. Du, Y. Zhang and S. Chen, Hydrotalcite-PLGA composite nanoparticles for loading and delivery of danshensu, *RSC Adv.*, 2020, **10**(37), 22010–22018.
14 Y. Cao, N. Mou, L. Zhu, *et al.*, Progress in the application of erythrocyte membrane biomimetic nanodrug carrier in atherosclerosis therapy, *Chin. J. Arterioscler.*, 2023, **31**(01), 1–8.
15 C. L. Domínguez-delgado, Z. Akhtar, G. Awuah-mensah, *et al.*, Effects of process and formulation parameters on submicron polymeric particles produced by a rapid emulsion-diffusion method, *Nanomaterials*, 2022, **12**(2), 229.
16 P. Saralkar, T. Araiwala and W. J. Geldenhuys, Nanoparticle formulation and *in vitro* efficacy testing of the mitoNEET ligand NL-1 for drug delivery in a brain endothelial model of ischemic reperfusion-injury, *Int. J. Pharm.*, 2020, **578**, 119090.
17 Y. Liang, R. Ding, H. Wang, *et al.*, Orally administered intelligent self-ablating nanoparticles: a new approach to improve drug cellular uptake and intestinal absorption, *Drug Delivery*, 2022, **29**(1), 305–315.
18 Y. Li, H. Gao, X. Ran, *et al.*, Study of absorption dynamics in the body intestine of dehydrocamel derivative DH-004, *Chin. J. Clin. Pharmacol.*, 2021, **37**(07), 878–882.
19 Z. Liu, Z. Jiang, L. Liu, *et al.*, Mechanisms responsible for poor oral bioavailability of paeoniflorin: role of intestinal

disposition and interactions with sinomenine, *Pharm. Res.*, 2006, **23**(12), 2768–2780.

20 S. Li, G. Li, H. Wu, *et al.*, Pharmacokinetics and tissue distribution study in adjuvant arthritis rats after oral administration of paeoniflorin by UHPLC-MS/MS, *Lat. Am. J. Pharm.*, 2016, **35**(5), 1011–1017.

21 Y. Tang, C. Gao, Y. Zhang, *et al.*, The microstructure and physiochemical stability of Pickering emulsions stabilized by chitosan particles coating with sodium alginate: influence of the ratio between chitosan and sodium alginate, *Int. J. Biol. Macromol.*, 2021, **183**, 1402–1409.

22 Y. Zhu, P. Sun, C. Duan, *et al.*, Improving stability and bioavailability of curcumin by quaternized chitosan coated nanoemulsion, *Food Res. Int.*, 2023, **174**(Pt 1), 113634.

23 C. Liu, Y. Yuan, M. Ma, *et al.*, Self-assembled composite nanoparticles based on zein as delivery vehicles of curcumin: role of chondroitin sulfate, *Food Funct.*, 2020, **11**(6), 5377–5388.

24 X. Wang, H. Lv, A. Y. Waddad, *et al.*, Study on intestinal absorption kinetics of gambogic acid in rats, *China J. Chin. Mater. Med.*, 2012, **37**(14), 2079–2083.

25 X. Wang, H. Lian, X. Lu, H. Y. Zheng, *et al.*, Intestinal absorption of phenolic acids in *Rhus chinensis* extracts by *in situ* single-pass perfusion model in rats, *China J. Chin. Mater. Med.*, 2019, **44**(11), 2373–2378.

26 W. Liu, H. Pan, C. Zhang, *et al.*, Developments in methods for measuring the intestinal absorption of nanoparticle-bound drugs, *Int. J. Mol. Sci.*, 2016, **17**(7), 1171.

27 Y. Mai, Y. Lin, J. Shi, *et al.*, Study on the effects of windproof extracts affecting the intestinal absorption of paeoniflorin, *Tradit. Chin. Drug Res. Clin. Pharmacol.*, 2021, **32**(09), 1338–1344.

28 J. N. Chu and G. Traverso, Foundations of gastrointestinal-based drug delivery and future developments, *Nat. Rev. Gastroenterol. Hepatol.*, 2022, **19**(4), 219–238.

29 S. Guo, Y. Liang, L. Liu, *et al.*, Research on the fate of polymeric nanoparticles in the process of the intestinal absorption based on model nanoparticles with various characteristics: size, surface charge and pro-hydrophobics, *J. Nanobiotechnol.*, 2021, **19**(1), 1–21.